JACS
JOURNAL OF THE AMERICAN CHEMICAL SOCIETY
pubs.acs.org/JACS
Article

Fe(deferasirox)$_2$: An Iron(III)-Based Magnetic Resonance Imaging T_1 Contrast Agent Endowed with Remarkable Molecular and Functional Characteristics

Lorenzo Palagi, Enza Di Gregorio, Diana Costanzo, Rachele Stefania, Camilla Cavallotti, Martina Capozza, Silvio Aime, and Eliana Gianolio*

Cite This: J. Am. Chem. Soc. 2021, 143, 14178−14188

Read Online

ACCESS | Metrics & More | Article Recommendations | Supporting Information

ABSTRACT: The search for alternatives to Gd-containing magnetic resonance imaging (MRI) contrast agents addresses the field of Fe(III)-bearing species with the expectation that the use of an essential metal ion may avoid the issues raised by the exogenous Gd. Attention is currently devoted to highly stable Fe(III) complexes with hexacoordinating ligands, although they may lack any coordinated water molecule. We found that the hexacoordinated Fe(III) complex with two units of deferasirox, a largely used iron sequestering agent, owns properties that can make it a viable alternative to Gd-based agents. Fe(deferasirox)$_2$ displays an outstanding thermodynamic stability, a high binding affinity to human serum albumin (three molecules of complex are simultaneously bound to the protein), and a good relaxivity that increases in the range 20−80 MHz. The relaxation enhancement is due to second sphere water molecules likely forming H-bonds with the coordinating phenoxide oxygens. A further enhancement was observed upon the formation of the supramolecular adduct with albumin. The binding sites of Fe(deferasirox)$_2$ on albumin were characterized by relaxometric competitive assays. Preliminary *in vivo* imaging studies on a tumor-bearing mouse model indicate that, on a 3 T MRI scanner, the contrast ability of Fe(deferasirox)$_2$ is comparable to the one shown by the commercial Gd(DTPA) agent. ICP-MS analyses on blood samples withdrawn from healthy mice administered with a dose of 0.1 mmol/kg of Fe(deferasirox)$_2$ showed that the complex is completely removed in 24 h.

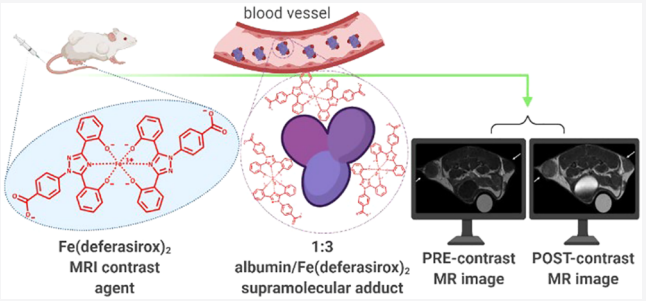

INTRODUCTION

Paramagnetic metal complexes were early identified as MRI contrast agents (CAs) for their ability to increase the relaxation rate of water protons in the regions where they distribute.[1−3] This property is assessed *in vitro* by measuring the relaxivity, i.e., the increase of the relaxation rate in the presence of 1 mM concentration of the metal complex. The paramagnetic ion of choice was the Gd^{3+} ion because of the high number of unpaired electrons (seven) and the relatively long electronic relaxation time. Therefore, Gd(III) complexes with linear and macrocyclic octadentate ligands were early selected, and nowadays about 40% of the clinical MRI scans make use of them. Their use is specifically recommended for the detection of small tumor lesions and for assessing liver abnormalities. The clinically used gadolinium-based contrast agents (GBCAs) are commonly administered intravenously at doses of 0.1 mmol/kg of patient weight. They were considered among the safest chemicals, but this statement has been recently challenged by two clinical observations, namely, (i) in the presence of renal impairment, a pathological condition (nephrogenic systemic fibrosis, NSF) was associated with the use of GBCAs, and (ii) tiny amounts of Gd-containing species were detected in the brain of patients, without evidence of renal excretion problems, undergone to the administration of one or more doses of GBCAs.[4−8] Although the latter observation has not been associated with any clinical consequence, it has nevertheless generated concern and prompted the probes' developers to actively tackle research activities for seeking possible alternatives to GBCAs.[9−12] In the field of the relaxation enhancers, it has been rather straightforward to look at endogenous paramagnetic metal ions, such as Mn(II) or Fe(III), on the basis of the expectation that their homeostasis in living cells and organisms would allow avoidance of *in vivo* accumulation.[11] Actually, high kinetic and thermodynamic stabilities are still considered basic requisites for complexes based on endogenous metal ions. Regarding Fe(III) complexes, besides the request of stability (as the lack of any interference with the endogenous iron pool

Received: May 13, 2021
Published: August 25, 2021

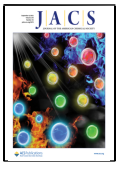

https://doi.org/10.1021/jacs.1c04963
J. Am. Chem. Soc. 2021, 143, 14178−14188

is considered an obvious advantage), one must avoid ROS-induced toxicity associated with iron redox cycling. This event normally occurs in systems with not sufficiently negative Fe(III)/Fe(II) redox potentials (i.e., higher than −0.2 V).[13] Moreover, it was suggested that systems containing coordinated water molecules can facilitate redox chemistry processes at the metal center with the consequent formation of harmful oxygen-based radicals.[14] The latter condition is of course a limitation for the intended application as one cannot exploit the contribution to the relaxivity arising from water molecules in the inner coordination sphere that, on the basis of what known from the extensive studies carried out on GBCAs, represents an important source to the observed relaxation enhancement. In spite of the fact that most of the Fe(III) complexes can rely only on the contribution of water molecules in the second and outer coordination spheres, they are currently under intense scrutiny as potential MRI CAs.[13,15−19] Interesting systems based on biodegradable iron containing macromolecules, such as melanoidin and polycatechol nanoparticles, have been proposed.[20,21] Among several possibilities, much attention has been devoted to the Fe(III) complexes bearing ligands that are represented by clinically approved iron sequestering agents.[22−24] It is expected that the large array of information available on the good biocompatibility of the Fe(III) complexes formed *in vivo* upon the administration of these ligands may provide a good support for facilitating their clinical translation as MRI CAs.

Herein, the *in vitro* and *in vivo* studies on Fe(deferasirox)$_2$ are reported. Deferasirox (DFX) is one of the most used iron sequestering agents in thalassemic patients.[25,26] It is administered orally and easily passes to blood where it tightly binds to human serum albumin (HSA). Upon its long circulation lifetime, DFX is ready to efficiently chelate the Fe^{3+} ions in excess in the anatomical regions where it is distributed, by the formation of a hexacoordinated Fe(III) complex with two units of ligand (chemical structure in Chart 1).

Chart 1. Chemical Structure of the Complex Fe(deferasirox)$_2$

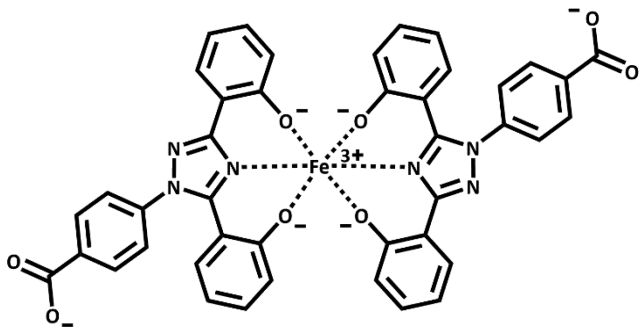

Interestingly, Fe(DFX)$_2$ displays four negatively charged oxygens in the inner coordination sphere which may provide a corresponding number of sites for the setup of H-bonded water molecules in the second coordination sphere. It is worth noting that the Fe−H distance for such H-bonded second sphere water molecules is expected to be only slightly longer than the one shown by protons on an inner sphere water molecule. Analogous to the ligand, its metal complex strongly binds to HSA.[27,28] The latter property appeared interesting for the intended application, as the formation of a supramolecular adduct may allow the exploitation of the relatively long electronic relaxation time of the Fe^{3+} ion to generate a high relaxivity agent. The thermodynamic stability of the complex Fe(DFX)$_2$ was reported to be extremely high (log B = 38.6),[29] and the excretion was shown to occur via the hepatobiliary and, to a lesser extent, the renal route.[30,31] As shown by previously reported speciation diagrams, at physiological pH, only the Fe(DFX)$_2$ bis complex is present.[32]

RESULTS

The three negatively charged $[Fe(DFX)_2]^{3-}$ complex is easily formed by mixing 1:2 amounts of $FeCl_3$ and deferasirox (4-[(3,5-bis(2-hydroxyphenyl)-1,2,4)triazol-1-yl]benzoic acid, DFX), as described in the Experimental Section. To improve the aqueous solubility, its salt with meglumine (*N*-methylglucamine, MGL) as counterion was prepared ($[Fe(DFX)_2]MGL_3$). In this paper, such compound was used for all the *in vitro* and *in vivo* experiments, and it is simply reported as Fe(deferasirox)$_2$ or Fe(DFX)$_2$.

***In Vitro* Relaxometric Investigations.** The relaxivity (r_1 and r_2) values measured at 298 and 310 K, at 0.47 and 1 T, and in water and in human serum are reported in Table 1. The

Table 1. Longitudinal and Transverse Relaxivities of Fe(DFX)$_2$[a]

medium	field (T)	T (K)	r_1 (mM^{-1} s^{-1})	r_2 (mM^{-1} s^{-1})
water	0.47	298	2.5 ± 0.31	2.9 ± 0.29
		310	1.7 ± 0.20	2.5 ± 0.22
	1	298	2.3 ± 0.22	3.1 ± 0.34
		310	1.4 ± 0.18	2.4 ± 0.21
human serum	0.47	298	3.4 ± 0.32	5.4 ± 0.35
		310	3.1 ± 0.25	5.1 ± 0.41
	1	298	4.4 ± 0.33	6.3 ± 0.29
		310	4.1 ± 0.41	6.6 ± 0.42

[a]Data measured in water and in human serum at 298 K and 310 K, at 0.47 T and 1 T, and at pH 7.4.

observed relaxivities remained unchanged over several days when the solutions were maintained at 310 K (Figure S6 of Supporting Information). The relaxivity of Fe(DFX)$_2$ was constant over the pH range 6−10 (Figure S7). Furthermore, the observed relaxivities decreased upon increasing the temperature to show that their values were not "quenched" by the occurrence of a slow exchange of the involved protons.

The absence of any contribution to the observed relaxivity arising from inner sphere water molecules coordinated to Fe(III) ion was assessed by carrying out the variable-temperature ^{17}O-T_2-NMR experiment, in analogy to what was first proposed by Snyder et al.[13] As shown in Figure 1, when the ^{17}O-T_2-NMR data obtained at 14.1 T for a 20 mM solution Fe(DFX)$_2$ are compared to those ones generated by two well-known complexes with q = 1 (Fe(CDTA)) and q = 0 (Fe(DTPA)), it is evident that Fe(DFX)$_2$ behaves as a q = 0 system.

More insights into the effect of the applied magnetic field strength on the observed longitudinal and transverse relaxivities were gained by measuring the NMRD profiles on a fast field cycling (FFC) relaxometer (Figure 2).

In the cases of Gd(III) and Mn(II) based systems, NMRD profiles are commonly fitted to the values calculated on the basis of the Solomon−Bloembergen−Morgan (SBM) equations as, for these systems, it can be assumed that the Zeeman energy is much larger than the zero field splitting (ZFS)

https://doi.org/10.1021/jacs.1c04963
J. Am. Chem. Soc. 2021, 143, 14178−14188

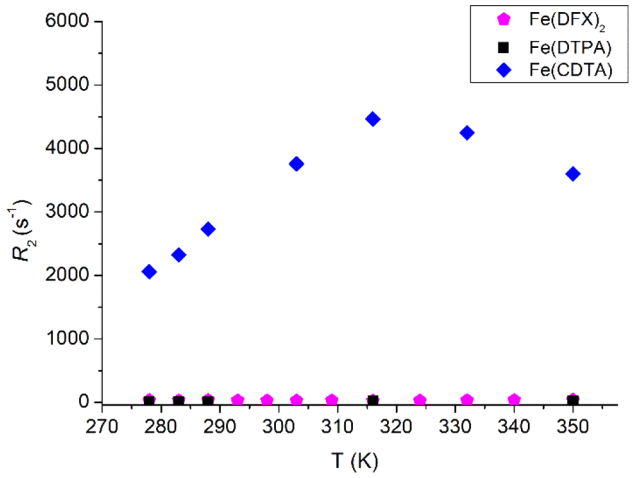

Figure 1. Comparison between $Fe(DFX)_2$, Fe(DTPA), and Fe(CDTA) ^{17}O-transverse relaxation rate measured as a function of temperature at 14.1 T and pH 7.4. Data are normalized to 20 mM iron concentration.

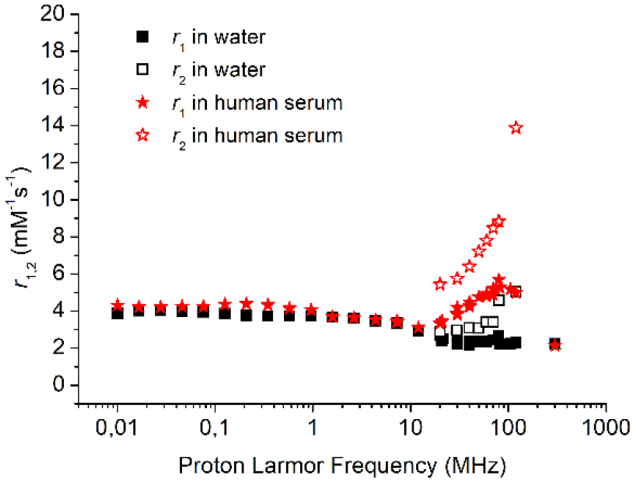

Figure 2. r_1 and r_2 NMRD profiles of $Fe(DFX)_2$ in water (black) and human serum (red) at 298 K and pH 7.4. Data are normalized to 1 mM iron concentration.

term.[33] Instead, for Fe(III)-based systems, SBM theory is likely not to be considered a valid approach given the high ZFS values reported for Fe(III) complexes.[34] Actually, not many examples of fitted NMRD profiles of iron-based systems have been reported in the literature.[35−38] Indeed, in a seminal paper from Bertini et al. the NMRD profiles of $Fe(OH)_6^{3+}$ were fitted on the basis of the values calculated from the SBM theory, but that was the case of a highly symmetric system where ZFS is likely to be negligible. In the $Fe(DFX)_2$ complex, the asymmetry introduced by substituting the six oxygens of coordinating waters with four oxygens and two nitrogens from the coordinating ligand is likely to lead to an increase in ZFS in analogy to what occurs with other iron-based compounds.

Therefore, only qualitative considerations on the observed relaxivity data at variable magnetic field can be made for $Fe(DFX)_2$.

A key determinant for paramagnetic relaxation is represented by the number of exchanging protons that transfer the relaxation enhancement to the bulk water protons. In the case of paramagnetic complexes with $q = 0$ this role is ascribed to mobile protons present in the ligand or, more commonly, to the water molecules in the second coordination sphere. In $Fe(DFX)_2$ no labile protons are present on the ligand and, therefore, the observed relaxivity is determined by the occurrence of water molecules in the second coordination sphere. This assumption is certainly valid in water, but in the case of the experiment in serum, one may not rule out the occurrence of the contribution arising from exchanging protons on HSA at the binding interaction sites of $Fe(DFX)_2$.

The broad "hump" shown by $Fe(DFX)_2$ in serum in the high field region is determined by a complex interplay between the elongated τ_R, the electronic relaxation time (which increases with the magnetic field strength), and the exchange lifetime of second sphere water molecules. The latter exchange process is still fast on the NMR time scale as the relaxivity decreases upon increasing the temperature. The marked increase in r_1 from 0.5 to 2 T observed in serum appears consistent with the view that the occurrence of a tight interaction between $Fe(DFX)_2$ and HSA yields T_{1e} to become crucial in the determination of the observed relaxivity.

The binding strength to human serum albumin was investigated by measuring the relaxation enhancement of a phosphate buffer solution (PBS) of $Fe(DFX)_2$ upon the addition of increasing amounts of protein (Figure 3A). The number of binding sites on HSA can be better determined by

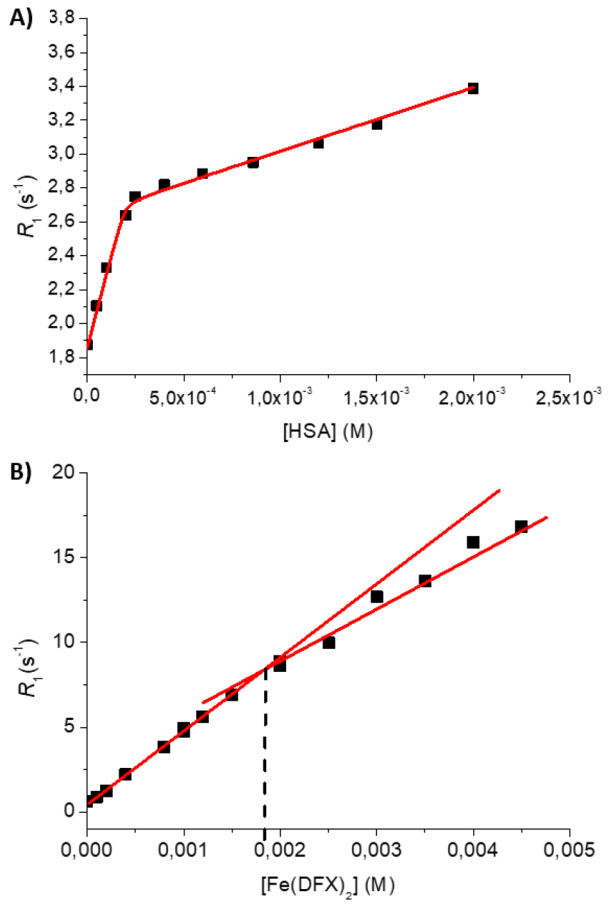

Figure 3. (A) Proton relaxation enhancement titration of $Fe(DFX)_2$ (0.56 mM) with increasing concentrations of HSA, in phosphate buffer, 298 K, 0.47 T. (B) Proton relaxation enhancement titration of HSA (0.6 mM) with increasing concentrations of $Fe(DFX)_2$, in phosphate buffer, 298 K, 0.47 T.

https://doi.org/10.1021/jacs.1c04963
J. Am. Chem. Soc. 2021, 143, 14178−14188

measuring the observed relaxation rate with a fixed concentration of HSA and an increasing concentration of the paramagnetic complex (Figure 3B).

The inflection point in Figure 3B indicates the ratio between $Fe(DFX)_2$ and HSA where the protein is saturated by the paramagnetic complex, and thus it provides direct evidence for the number of binding sites. Inspection into the experimental data indicates that three $Fe(DFX)_2$ units bind, with very high affinity, to one molecule of HSA as the inflection point is observed at [HSA] = 0.6 mM and $[Fe(DFX)_2]$ = 1.8 mM.

The titration reported in Figure 3A shows that the first aliquots of HSA bind almost quantitatively to the complex. The further increase in R_1 at higher concentrations of HSA reflects the protein diamagnetic contribution to relaxation and the increase in the overall viscosity. The fitting of the experimental data according to the proton relaxation enhancement equations (see Supporting Information) afforded, for the three binding sites, an average apparent binding constant (K_a) of 2.8×10^5 M^{-1} and a relaxivity of the HSA-bound complex (r_1^b) of 3.8 mM^{-1} s^{-1} at 0.47 T and 298 K.

More insights into the characterization of the binding sites were acquired by carrying out relaxometric experiments (Figure 4) in the presence of competitive ligands whose recognition abilities for specific binding sites on HSA are well-known.[39−42] The typical inhibitors used for each binding site were ibuprofen for subdomain IIIA (Sudlow site II), warfarin and iodipamide for subdomain IIA (Sudlow site I), and methyl orange for subdomain IB, respectively. Two inhibitors were tested for subdomain IIA, as previous studies on a HSA-binding Gd-complex have suggested that, due to the large size of the binding site, it is possible that warfarin and the paramagnetic complex can bind simultaneously, while the larger size of iodipamide can displace the Gd(III) complex.[43]

From these experiments (Figure 4A) it is clear that all the used competitors are able to yield a partial displacement of $Fe(DFX)_2$ from albumin. It follows that the binding sites are localized in the subdomains IB, IIA, and IIIA, following the well-established description of albumin recognition properties. However, from the data reported in Figure 4A, one may note that the asymptotic value at high concentration of the competing ligand is not the same for the three sites. R_1 is the lowest for methyl orange (IB) whereas the replacement of $Fe(DFX)_2$ at site IIA by warfarin or iodipamide and at site IIIA by ibuprofen yielded similar, higher R_1 values. Next, supplemental titrations were carried out in order to estimate the association constant of $Fe(DFX)_2$ for each albumin binding site. Three titrations of $Fe(DFX)_2$ with increasing concentration of albumin were carried out in the simultaneous presence of two of the competing drugs specific for the different principal binding sites (in a ratio of 1.5:1 with HSA) and leaving only one site free for $Fe(DFX)_2$ interaction (Figure 4B). Fitting each of these profiles with the same PRE equations used in Figure 3A allowed calculation of the association constant and the bound relaxivity (r_1^b) for the binding site not occupied by the competitors. It follows that addition of ibuprofen and iodipamide enabled the quantification of the apparent binding constant for site IB, ibuprofen and methyl orange for site IIA, and iodipamide and methyl orange for site IIIA. The following results were obtained: site IB, $K_a = 7.1 \times 10^4$ M^{-1} and r_1^b = 3.8 mM^{-1} s^{-1}; site IIA, $K_a = 5.9 \times 10^4$ M^{-1} and r_1^b = 3.5 mM^{-1} s^{-1}; site IIIA, $K_a = 1.9 \times 10^4$ M^{-1} and r_1^b = 3.2 mM^{-1} s^{-1}.

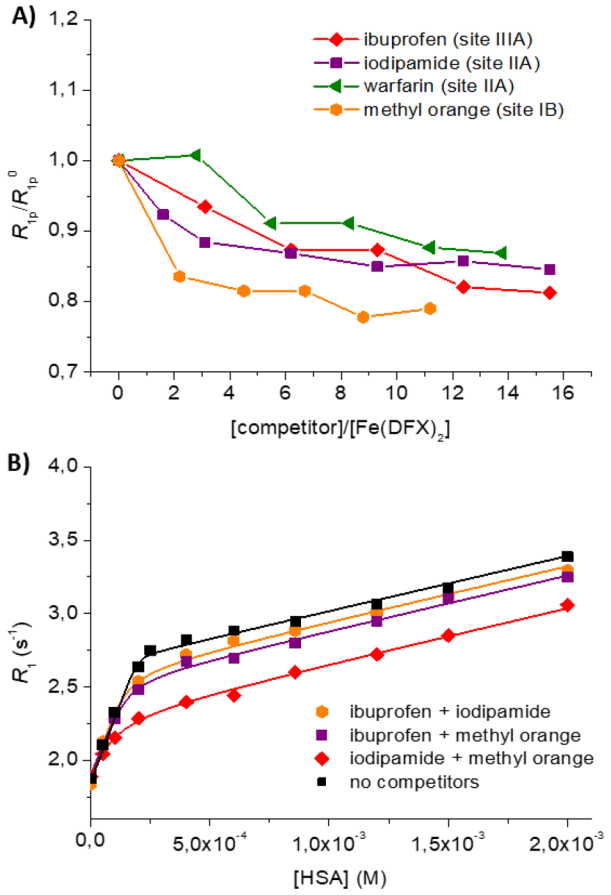

Figure 4. (A) Displacement of $Fe(DFX)_2$ from HSA as determined by the change in relaxivity as a function of increasing concentration of the added competitors relative to the respective binding site on HSA (298 K, 0.47 T, $[Fe(DFX)_2]$ = 0.6 mM, [HSA] = 0.2 mM in phosphate buffer). R_{1p}/R_{1p}^0 is the R_{1p} value of the solution normalized to the initial value (R_{1p}^0) without any inhibitor. $R_{1p} = R_{1obs} - R_{1d}$. (B) Proton relaxation enhancement titration of $Fe(DFX)_2$ (0.56 mM in phosphate buffer) with increasing concentrations of HSA, in the presence of couples of competitors (as detailed in the legend) in 1.5:1 ratio with respect to HSA (298 K, 0.47 T).

From this set of experiments, it can be concluded that sites IB and IIA are the strongest ones for $Fe(DFX)_2$ binding on albumin, while a slightly lower affinity has been observed for site IIIA. It must be noted that the K_a determined in the absence of any competing drug (Figure 3A) is approximately 4−5 times higher than the averaged K_a determined from the individual measurements for each binding site. This discrepancy can be likely ascribed to the fact that the competitors were added in excess (1.5 times) with respect to albumin. Whereas the latter choice was deemed necessary to push for a complete occupation of the given relative binding site, nevertheless it might give raise to unwanted effects in the determination of the respective K_a value.

The values obtained for the relaxivity of $Fe(DFX)_2$ bound to each of the three binding sites confirmed the qualitative trend reported in Figure 4A, as the highest r_1^b was observed for $Fe(DFX)_2$ bound to site IB followed by those relative to sites IIA and IIIA, respectively.

***In Vivo* Imaging Studies.** T_1-weighted MR images were acquired on a 3 T scanner. To get a reliable picture of the overall performance of $Fe(DFX)_2$ as MRI CA, the *in vivo* experiments were compared with the results obtained by

https://doi.org/10.1021/jacs.1c04963
J. Am. Chem. Soc. 2021, 143, 14178−14188

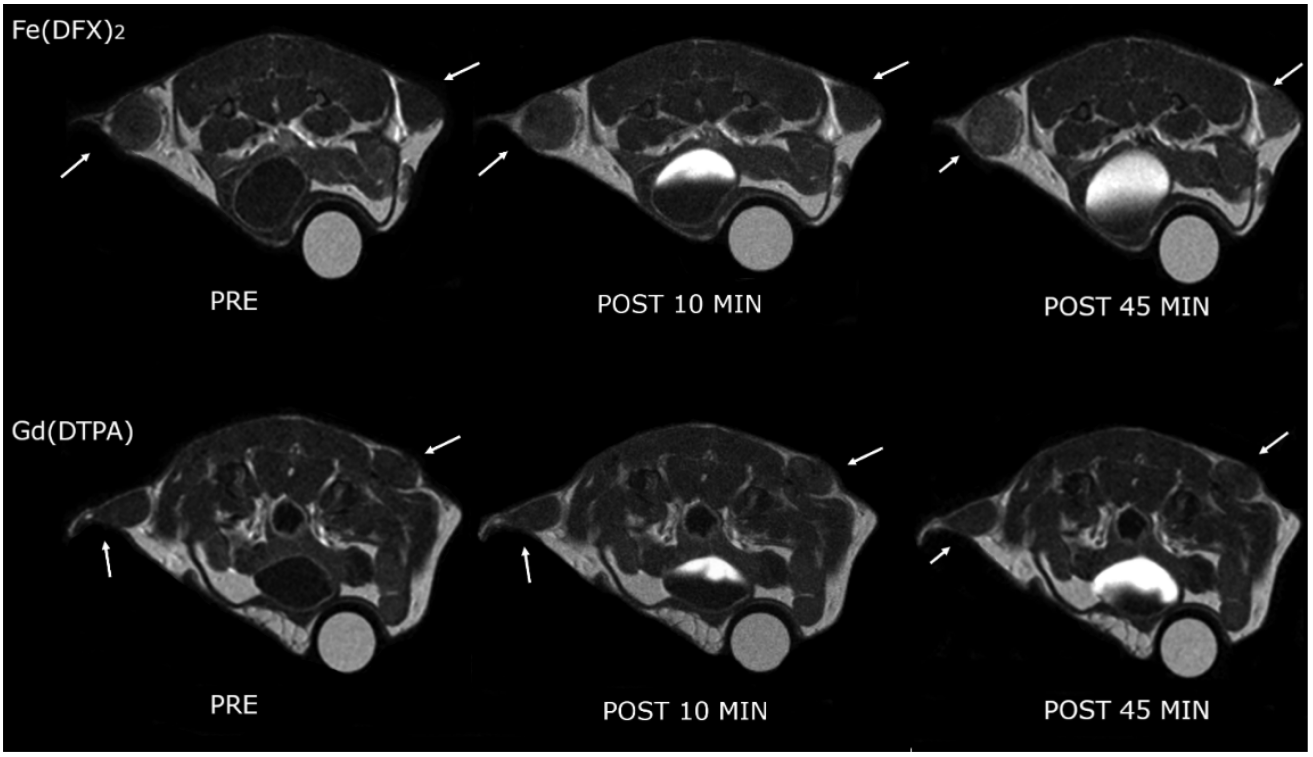

Figure 5. Representative MR T_1-weighted images of the TS/A-inoculated mouse pre- and post- (10 or 45 min) contrast agent administration ($Fe(DFX)_2$ and Gd(DTPA), 0.1 mmol/kg). The arrows indicate the tumor regions.

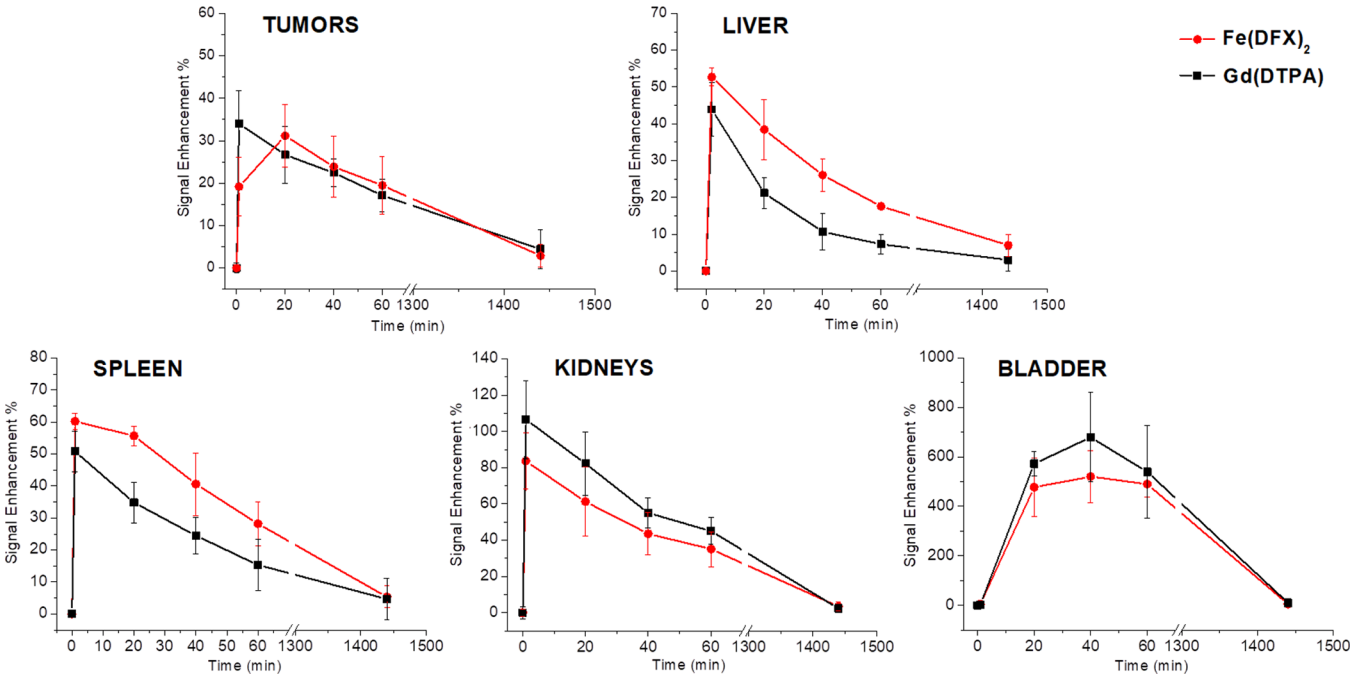

Figure 6. Comparison between the changes in signal enhancement over time in various body regions after the *in vivo* administration of a dose (0.1 mmol/kg) of $Fe(DFX)_2$ and Gd(DTPA).

administering Gd(DTPA) (Magnevist, gadopentetate dimeglumine) on the same mouse models at the same dose of 0.1 mmol/kg. At 3 T, Gd(DTPA) displays an *in vitro* relaxivity value, in water, not much different from $Fe(DFX)_2$.[15]

The *in vivo* experiments were carried out on mice (n = 6) bearing a TS/A breast tumor xenograft. In Figure 5 representative MR T_1-weighted images of the TS/A-inoculated mouse pre- and postcontrast ($Fe(DFX)_2$ and Gd(DTPA) are reported. Details on the changes in the signal intensities (SI) for the tumor regions and for selected organs are reported in Figure 6.

In general, one may state that the contrast enhancement behaviors shown by $Fe(DFX)_2$ and Gd(DTPA) were rather similar. Also, the wash-out kinetics as assessed by the return of

https://doi.org/10.1021/jacs.1c04963
J. Am. Chem. Soc. 2021, 143, 14178−14188

the SI at the precontrast values were shown to be rather similar.

Assessment of the Elimination of $Fe(DFX)_2$ Complex from Blood. The rates of elimination of $Fe(DFX)_2$ or Gd(DTPA) from blood of healthy mice intravenously administered with 0.1 mmol/kg of contrast agent were determined through the ICP-MS analyses of Fe or Gd in blood samples collected from mice at different time points (Figure 7).

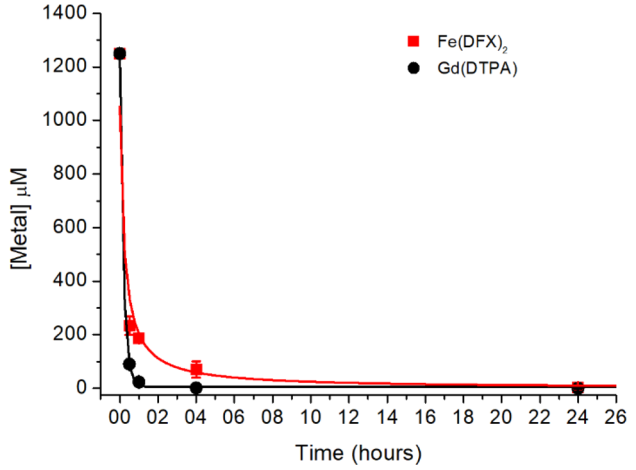

Figure 7. Curves representing the decrease of the exogeneous Fe and Gd concentrations from the blood of healthy mice upon the intravenous administration of a dose (0.1 mmol/kg) of $Fe(DFX)_2$ or Gd(DTPA), respectively.

The plasma specimens were extracted from blood and mineralized following the procedure described in the Experimental Section. The amount of residual heme iron present in the plasma (because of an unavoidable occurring slight RBCs lysis) was calculated by acquiring UV−vis absorption spectra (λ = 413 nm, Soret band) and subtracted from the overall iron amount measured by ICP-MS. The decrease of $Fe(DFX)_2$ concentration in blood appeared to follow a slower kinetic with respect to that of Gd(DTPA).

The concentrations of total Fe and Gd in plasma were 16% and 1.6% of the initial blood metal concentrations (1.25 mM at t_0, calculated as 0.0025 administered mmol in 2 mL of mouse blood volume) at 1 h and 10% and 0.2% at 2 h after the administration, respectively. These values are fully consistent with those reported in a pharmacokinetic study carried out on $Fe(DFX)_2$ where 12% of the injected dose was determined 1 h after injection.[31] The slower elimination rate of $Fe(DFX)_2$ is indeed related to its blood-pool characteristics as albumin-binding agent.

DISCUSSION

The herein reported relaxation enhancement and the overall biodistribution/excretion properties of $Fe(DFX)_2$ make this system a potential alternative to the currently used GBCAs. On a 3 T scanner, the observed SI enhancements in the tumor region, and in other body organs, were comparable to those brought about by Gd(DTPA), one of the most clinically used GBCAs. By considering that the NMRD profiles showed a marked increase of the relaxivity in the 1−2 T range of magnetic field strength, $Fe(DFX)_2$ is expected to perform better than the current GBCAs at the most currently used field of 1.5 T available on clinical scanners.

Of course, one of the main advantages of $Fe(DFX)_2$ relies on its proven biocompatibility. The DFX ligand is daily used by a large number of thalassemic patients for its ability to extract iron ions that accumulate in their tissues upon the blood transfusions they need to undergo for their survival. Upon its action as a sequestering agent, DFX forms a highly stable complex with the metal ions provided by the iron pool. In the herein intended use, $Fe(DFX)_2$ is synthesized *in vitro* and administered intravenously. When circulating in the body, it behaves as the complex formed in the case of the use of DFX as therapeutic agent, i.e., without any risk of interference with the homeostasis of iron or other metal ions as its remarkably high stability warrants against any metal release. If the choice of using the clinically employed deferasirox as ligand to chelate Fe(III) can be seen as a forerunner of good biocompatibility properties, one has to consider the relevant differences from the clinical application of DFX and the herein suggested exploitation of $Fe(DFX)_2$ as relaxation enhancer. The iron chelator DFX is in fact administered orally with a daily dose of 5−40 mg/kg (0.013−0.1 mmol/kg) corresponding to a maximum plasma concentration (C_{max}) of 0.02−0.12 mM.[30] This range of values is well below the maximum concentration reached by GBCAs immediately after their intravenous injection. On the other hand, while the plasma concentration of GBCAs rapidly decreases after the injection, the prolonged retention in the bloodstream of $Fe(DFX)_2$, due to its high plasma protein binding, allows for maintaining its contrast effect for longer times. It follows that the use of $Fe(DFX)_2$ as MRI CA will have to be tailored to its peculiar properties.

In plasma, three units of $Fe(DFX)_2$ bind to one albumin. The involved sites on the protein were those classified as IB, IIA, and IIIA in the commonly accepted description of the HSA binding sites.[39−42] The competitive assays showed that the decrease of relaxation enhancement observed when $Fe(DFX)_2$ is replaced by the competing ligand is site-specific. In each experiment the attained relaxivity is, of course, the sum of the relaxation enhancement brought by the paramagnetic agent in the two noninvolved sites plus the contribution from the released $Fe(DFX)_2$. The observation that when the complex is displaced from the site IB, R_1 is the lowest implies that this site provides a large contribution to the overall r_1 of $Fe(DFX)_2$ bound to HSA. This conclusion is also supported by the values of r_1^b calculated when $Fe(DFX)_2$ is bound to each of the three binding sites, with IB > IIA > IIIA being the order of bound-relaxivities. This caveat may guide the design of site-specific binders to HSA for attaining higher relaxivities.

Furthermore, $Fe(DFX)_2$ is highly robust to any redox chemistry at the iron center. It is a very weak oxidizing agent (above pH 6, $E_{1/2}$ = −0.58 V), and reduction to $Fe(II)(DFX)_2$ is not anticipated under physiological conditions.[32]

Moreover, its stability further supports the view that it will not generate any toxicological issues. This property was also at the basis of the proposal of analogous approaches done by other groups in the use of highly stable metal complexes (including other sequestering agents such as deferoxamine).[22−24] The obvious advantage of $Fe(DFX)_2$ is its good relaxivity that is, in serum, the highest ever reported for a q = 0 Fe(III)-complex.

$Fe(DFX)_2$ binds very tightly to HSA to form a 3:1 supramolecular adduct. The binding to albumin appears to cause the structuring in the second coordination sphere proton

https://doi.org/10.1021/jacs.1c04963
J. Am. Chem. Soc. 2021, 143, 14178−14188

network. Likely, the second sphere water molecules are H-bonded at the negatively charged, coordinating phenoxide oxygens and their correlation time is affected by the lifetime of the undergoing H-bonds. In this context, it appears quite reasonable that the water molecules trapped in the supramolecular adduct with HSA are much less mobile than the water molecules in the free complex. It follows that the reorientational motion of the second sphere water molecules becomes relevant to determine the relaxivity enhancement when the magnetic field strength is increased. The exploitation of the lengthening of T_{1e} was a common practice in the case of slowly moving GBCAs displaying relaxivity peaks at around 1 T where the correlation times for the electronic relaxation of Gd(III) ions approach the value of the molecular reorientational time (for HSA bound complexes, τ_R is the range of 3−20 ns).[44,45] Very recently, a system based on a Fe(III) ion coordinated to three catecholate ligands bearing a rhodamine moiety on their surface was reported to display, through the binding to HSA, relaxometric enhancement properties similar to the ones herein reported for $Fe(DFX)_2$.[46]

As mentioned above, the assignment of the observed relaxation enhancement for $Fe(DFX)_2$ in serum to the closest protons on second sphere water molecules may represent an oversimplification as likely other mobile protons on the protein in the proximity of the interaction site may contribute. The involved protons (whatever is their origin) are in fast exchange with the bulk solvent as demonstrated by the decrease of the observed relaxivity upon the increase of the temperature. At 298 K, the relaxivity of the $Fe(DFX)_2$/HSA adduct is 3.8 mM^{-1} s^{-1} at 0.47 T, but it becomes 5.7 mM^{-1} s^{-1} at 2 T. It was reported that the tumor extracellular matrix (ECM) may be particularly rich in albumin as this protein is the main energy and nutrition source for tumor growth and it has been proposed as biomarker of cancer.[47] This may explain the good SI (and relatively long wash-out) shown by $Fe(DFX)_2$ in the tumor region.

Currently, the idea of using iron-based MRI CAs is actively pursued by radiologists through the off-label applications of ferumoxytol, a drug designed for supplying iron to anemia-patients. Ferumoxytol consists of ultrasmall superparamagnetic iron oxide nanoparticles (USPIONs) whose mediated proton relaxation rate enhancement is strongly dependent on compartmentalization of the agent.[48] There is an obvious analogy between the use of ferumoxytol and the herein proposed $Fe(DFX)_2$ approach as both aim to exploit systems that are already part of the clinical practice. Although the relaxation enhancement effect of ferumoxytol is definitively good, its intravascular confinement related to higher size makes ferumoxytol a poor choice as replacement for GBCAs because it could take hours to days for lesion enhancements.

CONCLUSIONS

$Fe(DFX)_2$ appears as a good candidate to be considered as an alternative to the currently used GBCAs because of its high biocompatibility profile shown upon its *in vivo* formation when DFX is used as an iron-sequestering agent. Our work added $Fe(DFX)_2$ with important relaxometric and imaging properties that are at least equivalent but, at the magnetic field strength of 1.5 T, possibly even superior to those shown by the clinically used GBCAs. Furthermore, one may think of designing other systems based on the coordination cage of DFX with the introduction of substituents that may allow an improved control of the mobility of the second sphere water molecules, thus maintaining the interesting field-dependent properties shown by $Fe(DFX)_2$.

EXPERIMENTAL SECTION

General. Deferasirox was purchased from Advanced Chemblocks Inc. Magnevist (gadopentetate dimeglumine, Gd(DTPA)) was purchased from Bayer S.p.A. All the other chemicals were purchased from Sigma-Aldrich Co. and were used without further purification. pH measurements were made using an AS pH meter equipped with a glass electrode. Chromatographic purification was performed using an AKTA purifier equipped with a UV-900 system, P-900 pump, frac-920 fraction collector, and a Sephadex G-10 resin column. Mass spectra were recorded on a Waters 3100 mass detector (direct infusion with H_2O/CH_3OH 2:1). HPLC analyses were carried out on a HPLC-Waters Alliance separation module with a 2998 PDA detector.

Synthesis of Iron Complexes. *$[Fe(deferasirox)_2]^{3-}$.* An amount of 75 mg (0.2 mmol, MW = 373.73) of 4-(3,5-bis(2-hydroxyphenyl)-1,2,4-triazol-1-yl)benzoic acid (deferasirox, DFX) was suspended in water (100 mL), basified to pH 9 with a 5 M aqueous solution of *N*-methyl-D-glucamine (meglumine, MGL), and heated at 60 °C under magnetic stirring until complete dissolution. An amount of 3.04 mL of a 25 mM aqueous solution of $FeCl_3$ (0.076 mmol) was added dropwise while maintaining pH 8 with MGL 5 M. The mixture was heated at 60 °C for 1 h under magnetic stirring. The product was purified by chromatography on Sephadex G-10 resin using water as eluent. The fraction containing the pure product was evaporated and freeze-dried. An amount of 75 mg of a red solid was obtained. Anal. Calcd for $C_{63}H_{77}FeN_9O_{23}\cdot 5H_2O$: C, 51.33; H, 5.95; N, 8.55. Found: C, 51.47; H, 5.72; N, 8.59.

The product was also analyzed by adjusting a method reported in literature[43] on a HPLC-Waters Alliance separation module with a 2998 PDA detector and using an Atlantis RP-C18 column. Eluent: 35% buffer (ammonium acetate 50 mM, tetrabutylammonium hydrogen sulfate 10 mM), 45% methanol, 20% acetonitrile. Wavelengths: 225 and 467 nm. Retention time: 2.7 min (Figures S2 and S3).

Mass spectra in direct infusion yielded $C_{42}H_{27}FeN_6O_8$ ESI-MS (−): *m*/*z* calcd 798.13 $[M - H]^-$, found 798.34; *m*/*z* calcd 398.58 $[M - 2H]^{2-}$, found 398.76 (Figure S1).

The speciation diagrams for $Fe(H_nDFX)_n$ at three different metal/ligand concentrations (20 μM/40 μM; 200 μM/400 μM; 1 mM/2 mM) reported in Figure S4 were made by HYDRA and MEDUSA programs.[49]

$[Fe(DTPA)]^{2-}$ and $[Fe(CDTA)]^-$. The meglumine salts of the complexes were prepared following the procedures reported in literature and dissolved in neat water for the ^{17}O-R_2-NMR experiments.[15]

Relaxometric Measurements. Observed longitudinal relaxation rates ($R_{1obs} = 1/T_{1obs}$) values were determined by inversion recovery at 21.5 MHz and 25 °C using a Stelar SpinMaster spectrometer (Stelar s.r.l, Mede (PV), Italy). Temperature was controlled with a Stelar VTC-91 airflow heater and the temperature inside the probe checked with a calibrated RS PRO RS55-11 digital thermometer. Data were acquired using a recovery time of $\geq 5 \times T_1$ and with 2 scans per data point. The absolute error in R_{1obs} measurements was less than 1%.

R_2 values were measured by using the Carr−Purcell−Meiboom−Gill (CPMG) sequence on a Bruker WP80 NMR electromagnet (21.5−80 MHz). Data were acquired using echo delay of 8000 ms and with 4 scans per data point.

The iron concentration of the investigated solutions of the $Fe(DFX)_2$ complex was determined by the procedure reported in literature.[50] The iron complex containing solutions were mixed in a 1:10 ratio with 69% HNO_3 and heated in sealed vials at 120 °C overnight to yield a solution of Fe^{3+} aqua ion. The R_{1obs} of the solution was measured at 298 K and 21.5 MHz and the concentration determined using the equation $R_{1obs} = R_{1d} + r_{1p}^{Fe}[Fe]$, where R_{1d} is the diamagnetic contribution (0.48 s^{-1}) and r_{1p}^{Fe} is the Fe^{3+} aqua ion relaxivity (18.47 mM^{-1} s^{-1}) under the same experimental conditions.

https://doi.org/10.1021/jacs.1c04963
J. Am. Chem. Soc. 2021, 143, 14178−14188

The iron concentration of the complexes was confirmed by ICP-MS analysis.

Longitudinal relaxivity (r_1) values reported in Table 1 were calculated as slope of the lines correlating observed relaxation rates measured at pH = 7.4, 298 K, or 310 K (0.47 T or 1 T) as a function of $Fe(DFX)_2$ concentration. An example (298 K, 0.47 T) of these plots is reported in Supporting Information (Figure S5).

Stability experiments were performed measuring the R_{1obs} values at 25 °C and 21.5 MHz over several days, while the phosphate buffer and human serum solutions of the complex were stored in sealed tubes at 37 °C.

The interaction of the iron complex to human serum albumin (HSA) was studied using the proton relaxation enhancement (PRE) method (equations in Supporting Information). Namely, the apparent binding constant (K_a) and the relaxivity of the adduct (r_1^b) were determined by measuring R_1 values of $Fe(DFX)_2$ (0.56 mM) as a function of increasing HSA concentration (0.05−2 mM) in PBS at 298 K, 21.5 MHz, pH 7.4 (Figure 3A). On the other hand, the number of binding sites was identified through the relaxometric titration of albumin solutions, at a fixed concentration of 0.6 mM, with increasing $Fe(DFX)_2$ concentrations (0.02−4.5 mM), Figure 3B.

Two sets of competitive experiments were carried out for the identification and characterization of the binding sites on human serum albumin. For the experimental data reported in Figure 4A, the R_1 values of solutions containing $Fe(DFX)_2$ (0.6 mM) and HSA (0.2 mM) as a function of increasing concentration of the added competitors were measured in PBS at pH 7.4, 298 K, 21.5 MHz. For the titrations reported in Figure 4B, R_1 values were measured for solutions of $Fe(DFX)_2$ (0.56 mM) as a function of increasing HSA concentration (0.05−2 mM) in the presence of pairs of competitors in a ratio 1.5:1 toward HSA in PBS at pH 7.4, 298 K, 21.5 MHz.

NMRD Profiles. NMRD profiles were obtained using a Stelar SpinMaster FFC NMR relaxometer from 0.01 to 20 MHz. Additional data in the 20−120 MHz frequency range were obtained with a high field relaxometer (Stelar) equipped with the HTS-110 3 T metrology cryogen-free superconducting magnet and a Bruker WP80 NMR electromagnet (21.5−80 MHz), both equipped with a Stelar VTC-91 for temperature control; the temperature inside the probe was checked with a calibrated RS PRO RS55-11 digital thermometer. Aqueous and human serum solutions of the complex were measured at 25 and 37 °C.

^{17}O-R_2-NMR Measurements. O^{17}-NMR measurements were recorded at 14.1 T on a Bruker Avance 600 spectrometer at variable temperature, with a D_2O capillary for sample locking. Samples contained 1% of $H_2{}^{17}O$ (Cambridge Isotope) and the Fe(III) complexes (20 mM $Fe(DFX)_2$, 20 mM Fe(DTPA), and 4.5 mM Fe(CDTA)). The width at half-maximum ($\Delta\omega_{dia}$) of the $H_2{}^{17}O$ signal in pure water was measured over the investigated temperature range and subtracted from the width at half-maximum ($\Delta\omega_{Fe}$) of the test solutions containing the Fe-complexes. Then, R_2 was calculated as follows: $R_2 = \pi[\Delta\omega_{Fe} - \Delta\omega_{dia}]$. To compare the different profiles, R_2 values were normalized to 20 mM concentration of Fe(III)-complex.

Cell Culture and Animals. TS/A murine breast cancer cells were derived at the University of Torino from a spontaneous mammary adenocarcinoma which arose in a retired breeder BALB/c female. They were grown in RPMI (Roswell Park Memorial Institute) 1064 medium supplemented with 10% heat-inactivated fetal bovine serum (FBS), 2 mM glutamine, 100 U/mL penicillin, and 100 μg/mL streptomycin. Cells were seeded in 75 cm^2 flasks at density of approximately 5×10^4 cells/cm^2 in a humidified 5% CO_2 incubator at 37 °C. At confluence, they were detached by adding 1 mL of trypsin−EDTA solution (0.25% (w/v) trypsin-−0.53 mM EDTA). Cells were negative for mycoplasma as tested by using the MycoAlert mycoplasma detection kit. Cell media and supplements (RPMI, FBS, glutamine, pen/strep, MycoAlert mycoplasma detection kit) were purchased from Lonza Sales AG-EuroClone SpA, Milano (IT). *In vivo* experiments were carried out by using 10-week-old female Balb/C mice (Charles River Laboratories, Calco, Italy). Mice were kept in standard housing (12 h light/dark cycle) with rodent chow and water available ad libitum. Experiments were performed according to the Amsterdam Protocol on Animal Protection and in conformity with institutional guidelines that are in compliance with national laws (D.L.vo 116/92, D.L.vo 26/2014, and following additions) and international laws and policies (2010/63/EU, EEC Council Directive 86/609, OJL 358, Dec 1987, NIH Guide for the Care and Use of Laboratory Animals, U.S. National Research Council, 1996). This study was carried out in the framework of a protocol approved by the Italian Ministry of Health (authorization number 808/2017-PR). For tumor-model preparation, mice were anesthetized via an intramuscular injection of tiletamine/zolazepam (Zoletil 100; Virbac, Milan, Italy) 20 mg/kg plus xylazine (Rompun; Bayer, Milan, Italy) 5 mg/kg using a 27-gauge syringe. Approximately 3×10^5 TS/A cells were suspended in 0.1 mL of phosphate buffer solution and subcutaneously injected into each leg of mice ($n = 6$). Two tumors were implanted into each mouse to double the number of analyzed tumors. Animals were weekly monitored by calipers for changes in tumor size.

MRI Acquisition and Data Analysis. MR images were acquired 15 days after the tumor inoculation, with tumor dimension in a range of 80−120 mm.[3] For administration of Gd(DTPA) (0.1 mmol/kg) or $Fe(DFX)_2$ (0.1 mmol/kg) an intravenous catheter was inserted in the tail vein of the animal under anesthesia, before positioning inside the MR scanner. MR images were acquired with a Bruker BioSpec 3T MRI GmbH scanner (Bruker Biospin, Ettlingen, Germany) equipped with a 30 mm ^1H quadrature coil at room temperature (RT = 21 °C). T_{1W} images were acquired using a standard multislice multiecho sequence with the following parameters: repetition time (TR) 200 ms; echo time (TE) 11 ms; flip angle = 180°, number of averages = 4, field of view (FOV) 30 mm × 30 mm, slice thickness 1 mm; matrix size, 256 × 256. T_{2W} images were acquired using a standard RARE (rapid acquisition with refocused echoes) sequence with the following parameters: TR 3000 ms; TE 12 ms; FOV 30 mm × 30 mm; slice thickness 1 mm, flip angle = 180°, number of averages = 4, RARE factor 32; matrix size 256 × 256. A series of T_1-weighted MSME scans were acquired before and after the intravenous administration of the contrast agents to follow the kinetics of biodistribution.

The T_1 contrast enhancement (T_1 enh %) was calculated as follows:

$$SE\,\% = \frac{\left(\frac{SI(ROI)post}{SI(muscle)post}\right) - \left(\frac{SI(ROI)pre}{SI(muscle)pre}\right)}{\left(\frac{SI(ROI)pre}{SI(muscle)pre}\right)} \times 100$$

where SI(ROI)post and SI(ROI)pre are the signal intensities in the regions of interest (both normalized by dividing for signal intensity in muscle taken as reference) post- and preinjection of both contrast agents.

Assessment of the Elimination of $Fe(DFX)_2$ Complex from Blood. The kinetics of $Fe(DFX)_2$ and Gd(DTPA) removal from the blood were assessed by ICP-MS quantification of the Gd and Fe content in the plasma. For this purpose, after the intravenous injection of one dose (0.1 mmol/kg) of $Fe(DFX)_2$ or Gd(DTPA) to healthy mice ($n = 3$ for each time point), blood was collected from mice tail veins at variable time points (t = 30 min, 1 h, 4 h, 24 h). Blood was centrifuged for 7 min at 2300 rpm, RT, to separate and collect the plasma fraction.

An aliquot of plasma was used for measurement of Gd or overall (heme and not-heme) Fe by inductively coupled plasma mass spectrometry (ICP-MS). Another part was used for quantification of heme iron by UV−vis spectroscopy through the measure of the absorbance at λ = 413 nm (Soret band) by using a 6715 UV−vis spectrophotometer Jenway (Bibby Scientific Limited, Beacon Road, Stone, Staffordshire, ST15 OSA, U.K.). The heme iron concentration was calculated based on a previously obtained calibration curve in which the absorbance at λ = 413 nm was plotted against the iron concentration measured by ICP-MS in plasma samples collected from mice which were never received $Fe(DFX)_2$ (Figure S8).

Before ICP-MS analysis, plasma samples were digested with concentrated HNO_3 (70%) under microwave heating (Milestone MicroSYNTH microwave lab-station, Milestone Inc., Bergamo, Italy).

https://doi.org/10.1021/jacs.1c04963
J. Am. Chem. Soc. 2021, 143, 14178−14188

After the digestion, an amount of 2 mL of ultrapure water was added to each sample. The specimens were then subjected to ICP-MS analysis (Element-2; Thermo-Finnigan, Rodano (MI), Italy) to measure the concentration of Fe and Gd with respect to standard curves. The total iron content was subtracted by the heme iron to assess the effective plasma concentration of iron derived from $Fe(DFX)_2$ complex.

■ ASSOCIATED CONTENT

Supporting Information

The Supporting Information is available free of charge at https://pubs.acs.org/doi/10.1021/jacs.1c04963.

Chromatographic analysis and mass spectrum of $Fe(DFX)_2$, variation of the observed relaxation rate at 0.47 T, 298 K, and neutral pH of solutions with increasing concentration of $Fe(DFX)_2$ in the range 0.2−3.5 mM, relaxometric assessment of $Fe(DFX)_2$ stability in phosphate buffer and serum, variation of the relaxivity as a function of pH in the range 6−10, calibration curve of the absorbance at λ = 413 nm against the iron concentration measured by ICP-MS, and proton relaxation enhancement fitting equations (PDF)

■ AUTHOR INFORMATION

Corresponding Author

Eliana Gianolio − *Department of Molecular Biotechnology and Health Sciences, University of Torino, Torino 10126, Italy;* orcid.org/0000-0002-7130-4445; Email: eliana.gianolio@unito.it

Authors

Lorenzo Palagi − *Department of Molecular Biotechnology and Health Sciences, University of Torino, Torino 10126, Italy;* orcid.org/0000-0002-7612-8057

Enza Di Gregorio − *Department of Molecular Biotechnology and Health Sciences, University of Torino, Torino 10126, Italy*

Diana Costanzo − *Department of Molecular Biotechnology and Health Sciences, University of Torino, Torino 10126, Italy*

Rachele Stefania − *Department of Molecular Biotechnology and Health Sciences, University of Torino, Torino 10126, Italy*

Camilla Cavallotti − *CAGE Chemicals, Novara 28100, Italy*

Martina Capozza − *Department of Molecular Biotechnology and Health Sciences, University of Torino, Torino 10126, Italy*

Silvio Aime − *Department of Molecular Biotechnology and Health Sciences, University of Torino, Torino 10126, Italy; IRCCS SDN, Napoli 80143, Italy*

Complete contact information is available at: https://pubs.acs.org/10.1021/jacs.1c04963

Author Contributions

The manuscript was written through contributions of all authors. All authors have given approval to the final version of the manuscript.

Notes

The authors declare the following competing financial interest(s): C.C. is an employee of the company Cage Chemicals and holder of a patent on Fe(deferasirox)2 as MRI contrast agent.

■ ACKNOWLEDGMENTS

The authors acknowledge Prof. Mauro Botta and Dr. Fabio Carniato for recording NMRD profiles data in the frequency range 20−120 MHz. The authors acknowledge the Italian Ministry of Research for FOE contribution to the Euro-BioImaging MultiModal Molecular Imaging Italian Node (www.mmmi.unito.it). This research was performed in the framework of COST Action AC15209 (EURELAX) and of the Italian Consortium of Research on Chemistry of Metals in Biological Systems (CIRCMSB). The abstract graphic and table of contents graphic were created with BioRender.com.

■ ABBREVIATIONS

DFX, deferasirox; DTPA, diethylenetriaminepentaacetic acid; CDTA, cyclohexylethylenediaminetetraacetic acid; HSA, human serum albumin; GBCA, gadolinium-based contrast agent; MRI, magnetic resonance imaging; PBS, phosphate buffer solution; PRE, proton relaxation enhancement; ROS, reactive oxygen species; SI, signal intensity

■ REFERENCES

(1) Wahsner, J.; Gale, E. M.; Rodríguez-Rodríguez, A.; Caravan, P. Chemistry of MRI Contrast Agents: Current Challenges and New Frontiers. *Chem. Rev.* **2019**, *119* (2), 957−1057.

(2) Pierre, V. C.; Allen, M. J.; Caravan, P. Contrast Agents for MRI: 30+ Years and Where Are We Going? *JBIC, J. Biol. Inorg. Chem.* **2014**, *19* (2), 127−131.

(3) Aime, S.; Botta, M.; Fasano, M.; Terreno, E. Lanthanide(III) Chelates for NMR Biomedical Applications. *Chem. Soc. Rev.* **1998**, *27* (1), 19−29.

(4) Yang, L.; Krefting, I.; Gorovets, A.; Marzella, L.; Kaiser, J.; Boucher, R.; Rieves, D. Nephrogenic Systemic Fibrosis and Class Labeling of Gadolinium-Based Contrast Agents by the Food and Drug Administration. *Radiology* **2012**, *265* (1), 248−253.

(5) Kanda, T.; Ishii, K.; Kawaguchi, H.; Kitajima, K.; Takenaka, D. High Signal Intensity in the Dentate Nucleus and Globus Pallidus on Unenhanced T1-Weighted MR Images: Relationship with Increasing Cumulative Dose of a Gadolinium-Based Contrast Material. *Radiology* **2014**, *270* (3), 834−841.

(6) Errante, Y.; Cirimele, V.; Mallio, C. A.; Di Lazzaro, V.; Zobel, B. B.; Quattrocchi, C. C. Progressive Increase of T1 Signal Intensity of the Dentate Nucleus on Unenhanced Magnetic Resonance Images Is Associated With Cumulative Doses of Intravenously Administered Gadodiamide in Patients With Normal Renal Function, Suggesting Dechelation. *Invest. Radiol.* **2014**, *49* (10), 685−690.

(7) McDonald, R. J.; McDonald, J. S.; Kallmes, D. F.; Jentoft, M. E.; Murray, D. L.; Thielen, K. R.; Williamson, E. E.; Eckel, L. J. Intracranial Gadolinium Deposition after Contrast-Enhanced MR Imaging. *Radiology* **2015**, *275* (3), 772−782.

(8) Kanal, E.; Tweedle, M. F. Residual or Retained Gadolinium: Practical Implications for Radiologists and Our Patients. *Radiology* **2015**, *275* (3), 630−634.

(9) Fraum, T. J.; Ludwig, D. R.; Bashir, M. R.; Fowler, K. J. Gadolinium-Based Contrast Agents: A Comprehensive Risk Assessment. *Journal of Magnetic Resonance Imaging* **2017**, *46* (2), 338−353.

(10) Rogosnitzky, M.; Branch, S. Gadolinium-Based Contrast Agent Toxicity: A Review of Known and Proposed Mechanisms. *BioMetals* **2016**, *29* (3), 365−376.

(11) Tweedle, M. F. Alternatives to Gadolinium-Based Contrast Agents. *Invest. Radiol.* **2021**, *56* (1), 35−41.

(12) Wesolowski, J. R.; Kaiser, A. Alternatives to GBCA: Are We There Yet? *Topics in Magnetic Resonance Imaging* **2016**, *25* (4), 171−175.

(13) Snyder, E. M.; Asik, D.; Abozeid, S. M.; Burgio, A.; Bateman, G.; Turowski, S. G.; Spernyak, J. A.; Morrow, J. R. A Class of FeIII

Macrocyclic Complexes with Alcohol Donor Groups as Effective T1 MRI Contrast Agents. *Angew. Chem.* **2020**, *132* (6), 2435−2440.
(14) Graf, E.; Mahoney, J. R.; Bryant, R. G.; Eaton, J. W. Iron-Catalyzed Hydroxyl Radical Formation. Stringent Requirement for Free Iron Coordination Site. *J. Biol. Chem.* **1984**, *259* (6), 3620−3624.
(15) Boehm-Sturm, P.; Haeckel, A.; Hauptmann, R.; Mueller, S.; Kuhl, C. K.; Schellenberger, E. A. Low-Molecular-Weight Iron Chelates May Be an Alternative to Gadolinium-Based Contrast Agents for T1-Weighted Contrast-Enhanced MR Imaging. *Radiology* **2018**, *286* (2), 537−546.
(16) Bales, B. C.; Grimmond, B.; Johnson, B. F.; Luttrell, M. T.; Meyer, D. E.; Polyanskaya, T.; Rishel, M. J.; Roberts, J. Fe-HBED Analogs: A Promising Class of Iron-Chelate Contrast Agents for Magnetic Resonance Imaging. *Contrast Media Mol. Imaging* **2019**, *2019*, 8356931.
(17) Asik, D.; Smolinski, R.; Abozeid, S. M.; Mitchell, T. B.; Turowski, S. G.; Spernyak, J. A.; Morrow, J. R. Modulating the Properties of Fe(III) Macrocyclic MRI Contrast Agents by Appending Sulfonate or Hydroxyl Groups. *Molecules* **2020**, *25* (10), 2291.
(18) Xie, J.; Haeckel, A.; Hauptmann, R.; Ray, I. P.; Limberg, C.; Kulak, N.; Hamm, B.; Schellenberger, E. Iron(III)-TCDTA Derivatives as MRI Contrast Agents: Increased T1 Relaxivities at Higher Magnetic Field Strength and PH Sensing. *Magn. Reson. Med.* **2021**, *85* (6), 3370−3382.
(19) Wang, H.; Jordan, V. C.; Ramsay, I. A.; Sojoodi, M.; Fuchs, B. C.; Tanabe, K. K.; Caravan, P.; Gale, E. M. Molecular Magnetic Resonance Imaging Using a Redox-Active Iron Complex. *J. Am. Chem. Soc.* **2019**, *141* (14), 5916−5925.
(20) Lee, M.-Y.; Choi, D.; Jang, M.-S.; Lee, J. H. Biocompatible and Biodegradable Fe3+−Melanoidin Chelate as a Potentially Safe Contrast Agent for Liver MRI. *Bioconjugate Chem.* **2018**, *29* (7), 2426−2435.
(21) Li, Y.; Huang, Y.; Wang, Z.; Carniato, F.; Xie, Y.; Patterson, J. P.; Thompson, M. P.; Andolina, C. M.; Ditri, T. B.; Millstone, J. E.; Figueroa, J. S.; Rinehart, J. D.; Scadeng, M.; Botta, M.; Gianneschi, N. C. Polycatechol Nanoparticle MRI Contrast Agents. *Small* **2016**, *12* (5), 668−677.
(22) Mino, Y.; Kitagaki, H.; Sasaki, M.; Ishii, K.; Mori, T.; Yamada, K.; Nagasawa, O. Characterization of Fe(III)-Deferoxamine and Mn(II)-Pectin as Magnetic Resonance Imaging Contrast Agents. *Biol. Pharm. Bull.* **1998**, *21* (12), 1385−1388.
(23) Worah, D.; Berger, A. E.; Burnett, K. R.; Howard, H.; Kanal, E.; Kendall, C.; Leese, P. T.; Lyons, K. P.; Ross, E.; Wolf, G. L.; Quay, S. C. Ferrioxamine as a Magnetic Resonance Contrast Agent Preclinical Studies and Phase I and II Human Clinical Trials. *Invest. Radiol.* **1988**, *23*, S281.
(24) Duewell, S.; WüTHRICH, R.; Von Schulthess, G. K.; Jenny, H. B.; Muller, R. N.; Moerker, T.; Fuchs, W. F. Nonionic Polyethylene Glycol-Ferrioxamine as a Renal Magnetic Resonance Contrast Agent. *Invest. Radiol.* **1991**, *26* (1), 50−57.
(25) Moukalled, N. M.; Bou-Fakhredin, R.; Taher, A. T. Deferasirox: Over a Decade of Experience in Thalassemia. *Mediterr. J. Hematol. Infect. Dis.* **2017**, *10* (1), e2018066.
(26) Shirley, M.; Plosker, G. L. Deferasirox: A Review of Its Use for Chronic Iron Overload in Patients with Non-Transfusion-Dependent Thalassaemia. *Drugs* **2014**, *74* (9), 1017−1027.
(27) Weiss, H. M.; Fresneau, M.; Camenisch, G. P.; Kretz, O.; Gross, G. In Vitro Blood Distribution and Plasma Protein Binding of the Iron Chelator Deferasirox (Icl670) and Its Iron Complex Fe-[Icl670]2 for Rat, Marmoset, Rabbit, Mouse, Dog, and Human. *Drug Metab. Dispos.* **2006**, *34* (6), 971−975.
(28) Dehghan, G.; Shaghaghi, M.; Sattari, S.; Jouyban, A. Interaction of Human Serum Albumin with Fe(III)−Deferasirox Studied by Multispectroscopic Methods. *J. Lumin.* **2014**, *149*, 251−257.
(29) Heinz, U.; Hegetschweiler, K.; Acklin, P.; Faller, B.; Lattmann, R.; Schnebli, H. P. 4-[3,5-Bis(2-Hydroxyphenyl)-1,2,4-Triazol-1-Yl]-Benzoic Acid: A Novel Efficient and Selective Iron(III) Complexing Agent. *Angew. Chem., Int. Ed.* **1999**, *38* (17), 2568−2570.
(30) Tanaka, C. Clinical Pharmacology of Deferasirox. *Clin. Pharmacokinet.* **2014**, *53* (8), 679−694.
(31) Bruin, G. J. M.; Faller, T.; Wiegand, H.; Schweitzer, A.; Nick, H.; Schneider, J.; Boernsen, K.-O.; Waldmeier, F. Pharmacokinetics, Distribution, Metabolism, and Excretion of Deferasirox and Its Iron Complex in Rats. *Drug Metab. Dispos.* **2008**, *36* (12), 2523−2538.
(32) Steinhauser, S.; Heinz, U.; Bartholomä, M.; Weyhermüller, T.; Nick, H.; Hegetschweiler, K. Complex Formation of ICL670 and Related Ligands with FeIII and FeII. *Eur. J. Inorg. Chem.* **2004**, *2004* (21), 4177−4192.
(33) Holz, M. L.; Banci, L. Bertini and C. Luchinat. Nuclear and Electron Relaxation. The Magnetic Nucleus-Unpaired Electron Coupling in Solution. VCH, Weinheim, New York, Basel, Cambridge, 1991, Pp. 216, DM 118. ISBN 3-527-28306-4. *Magn. Reson. Chem.* **1993**, *31* (13), S154−S154.
(34) Schaefle, N.; Sharp, R. NMR Paramagnetic Relaxation Due to the S=5/2 Complex, Fe(III)-(Tetra-p-Sulfonatophenyl)Porphyrin: Central Role of the Tetragonal Fourth-Order Zero-Field Splitting Interaction. *J. Chem. Phys.* **2005**, *122* (18), 184501.
(35) Bertini, I.; Capozzi, F.; Luchinat, C.; Xia, Z. Nuclear and Electron Relaxation of Hexaaquairon(3+). *J. Phys. Chem.* **1993**, *97* (6), 1134−1137.
(36) Koenig, S. H.; Brown, R. D.; Lindstrom, T. R. Interactions of Solvent with the Heme Region of Methemoglobin and Fluoro-Methemoglobin. *Biophys. J.* **1981**, *34* (3), 397−408.
(37) Koenig, S. H.; Brown, R. D. Relaxation of Solvent Protons by Paramagnetic Ions and Its Dependence on Magnetic Field and Chemical Environment: Implications for NMR Imaging. *Magn. Reson. Med.* **1984**, *1* (4), 478−495.
(38) Cardoso, B. de P.; Vicente, A. I.; Ward, J. B. J.; Sebastião, P. J.; Chávez, F. V.; Barroso, S.; Carvalho, A.; Keely, S. J.; Martinho, P. N.; Calhorda, M. J. Fe(III) SalEen Derived Schiff Base Complexes as Potential Contrast Agents. *Inorg. Chim. Acta* **2015**, *432*, 258−266.
(39) Sudlow, G.; Birkett, D. J.; Wade, D. N. The Characterization of Two Specific Drug Binding Sites on Human Serum Albumin. *Mol. Pharmacol.* **1975**, *11* (6), 824−832.
(40) Sudlow, G.; Birkett, D. J.; Wade, D. N. Further Characterization of Specific Drug Binding Sites on Human Serum Albumin. *Mol. Pharmacol.* **1976**, *12* (6), 1052−1061.
(41) Zsila, F. Subdomain IB Is the Third Major Drug Binding Region of Human Serum Albumin: Toward the Three-Sites Model. *Mol. Pharmaceutics* **2013**, *10* (5), 1668−1682.
(42) Fanali, G.; di Masi, A.; Trezza, V.; Marino, M.; Fasano, M.; Ascenzi, P. Human Serum Albumin: From Bench to Bedside. *Mol. Aspects Med.* **2012**, *33* (3), 209−290.
(43) Longo, D. L.; Arena, F.; Consolino, L.; Minazzi, P.; Geninatti-Crich, S.; Giovenzana, G. B.; Aime, S. Gd-AAZTA-MADEC, an Improved Blood Pool Agent for DCE-MRI Studies on Mice on 1 T Scanners. *Biomaterials* **2016**, *75*, 47−57.
(44) Dumas, S.; Jacques, V.; Sun, W.-C.; Troughton, J. S.; Welch, J. T.; Chasse, J. M.; Schmitt-Willich, H.; Caravan, P. High Relaxivity Magnetic Resonance Imaging Contrast Agents Part 1: Impact of Single Donor Atom Substitution on Relaxivity of Serum Albumin-Bound Gadolinium Complexes. *Invest. Radiol.* **2010**, *45* (10), 600−612.
(45) Jacques, V.; Dumas, S.; Sun, W.-C.; Troughton, J. S.; Greenfield, M. T.; Caravan, P. High-Relaxivity Magnetic Resonance Imaging Contrast Agents Part 2: Optimization of Inner- and Second-Sphere Relaxivity. *Invest. Radiol.* **2010**, *45* (10), 613−624.
(46) Maheshwaran, D.; Nagendraraj, T.; Balaji, T. S.; Kumaresan, G.; Kumaran, S. S.; Mayilmurugan, R. Smart Dual T1 MRI-Optical Imaging Agent Based on a Rhodamine Appended Fe(III)-Catecholate Complex. *Dalton Trans.* **2020**, *49* (41), 14680−14689.
(47) Baroni, S.; Ruggiero, M. R.; Bitonto, V.; Broche, L. M.; Lurie, D. J.; Aime, S.; Geninatti Crich, S. In Vivo Assessment of Tumour Associated Macrophages in Murine Melanoma Obtained by Low-

https://doi.org/10.1021/jacs.1c04963
J. Am. Chem. Soc. 2021, 143, 14178−14188

Field Relaxometry in the Presence of Iron Oxide Particles. *Biomaterials* **2020**, *236*, 119805.
(48) Aghighi, M.; Golovko, D.; Ansari, C.; Marina, N. M.; Pisani, L.; Kurlander, L.; Klenk, C.; Bhaumik, S.; Wendland, M.; Daldrup-Link, H. E. Imaging Tumor Necrosis with Ferumoxytol. *PLoS One* **2015**, *10* (11), e0142665.
(49) Puigdomenech, I. HYDRA (Hydrochemical Equilibrium-Constant Database) and MEDUSA (Make Equilibrium Diagrams Using Sophisticated Algorithms) Programs. Royal Institute of Technology, Sweden. https://www.kth.se/che/medusa/ (accessed Jul 29, 2021).
(50) Svenskaya, Y.; Garello, F.; Lengert, E.; Kozlova, A.; Verkhovskii, R.; Bitonto, V.; Ruggiero, M. R.; German, S.; Gorin, D.; Terreno, E. Biodegradable Polyelectrolyte/Magnetite Capsules for MR Imaging and Magnetic Targeting of Tumors. *Nanotheranostics* **2021**, *5* (3), 362−377.

https://doi.org/10.1021/jacs.1c04963
J. Am. Chem. Soc. 2021, 143, 14178−14188